Simulation of an EHD thruster in pure argon at low pressure.

Victor H. Granados[1], Mario J. Pinheiro[2], Paulo A. Sá[1]

[1]*Faculdade de Engenharia da Universidade do Porto - FEUP, Portugal*
[2]*Departamento de Física, Instituto Superior Técnico - IST Universidade de Lisboa, Portugal.*

EHD thrusters are a useful means to convert electric energy into kinetic energy. In our work we develop a theoretical (self-consistent) 2D model of an axisymmetric electrostatic plasma actuator for argon gas at low pressure. The discharge is sustained by secondary electron emission from the cathode, which is due to ion impacts on its surface. In order to avoid the short-circuit regime, we consider an RC series matching circuit when applying a voltage to the electrodes. Here we investigate mainly the current flow mechanism. We demonstrate that EHD flow can be simulated if appropriate boundary conditions are chosen.

1. Introduction

Electrohydrodynamic (EHD) thrusters are devices that produce thrust from the movement of a fluid using an electric field. The ionization and acceleration of the gas are carried out by the electric field alone. Two electrodes are placed at a certain distance with a significantly different curvature radius [4]. The latter consists of an asymmetric capacitor in which the electric field is more intense on the surface of the electrode with the smaller curvature radius (positive electrode), favouring corona effect to appear (see [3],[8]).

2. Background

EHD thrusters use corona effect or corona discharge for ionization of the gas. It is a nonuniform discharge that produces a nonequilibrium low-ionized plasma. The ionized particles are accelerated by the electric field present between the electrodes. The accelerating ions -on their way to the opposite electrode (grounded electrode)- collide with neutral gas particles, transferring momentum to them, thus creating a stream of gas between electrodes. The stream of ionized gas is usually called ionic wind and it is the responsible for thrust generation (See [2], [11]).

After the ionization process occurs, free electrons are directed towards, and absorbed by, the anode at a faster rate than the ions reach the cathode giving the mass difference between the species, thus the electroneutrality of the plasma get initially affected. The discharge is then balanced by a secondary electron emission from the cathode due to ion impacts on its surface. The release of such electrons depends on both the ions species and the cathode's material (represented by the secondary electron emission coefficient, γ_i) and represents the key mechanism to sustain the discharge.

3. Model

The electric field is computed by solving the well-known Poisson equation,

$$\boldsymbol{\varepsilon \nabla^2 V = -e\left(\sum_{j=1}^{N} Z_j n_j - n_e\right)} \qquad (1)$$

where $\boldsymbol{\varepsilon}$ is the plasma permittivity, $\boldsymbol{Z_j}$ is the charge number of ions, $\boldsymbol{n_j}$ and $\boldsymbol{n_e}$ are the ions and electron densities, respectively [7].

For finding the rate coefficients of the electron-impact reactions

$$\boldsymbol{k_j = \left(\frac{2e}{m_e}\right)^{1/2} \int_0^{\infty} u\sigma_j(u) f(u) du} \qquad (2)$$

we assume a Maxwellian distribution function, where $\boldsymbol{u}$ is the electron energy (eV) and $\boldsymbol{\sigma_j(u)}$ is the elastic and inelastic (excitation and ionization) cross sections considered.

Compressible flow Navier-Stokes equations are used to obtain the velocity field and pressure distribution over the domain, including the bulk force $\boldsymbol{\vec{f} = \rho_c \vec{E}}$, where $\boldsymbol{\rho_c}$ is the space-charge density which is defined as the right side of equation (1).

An RC series coupling circuit is used when applying the voltage between the electrodes so the current flowing between the electrodes does not reach the arc regime (see figure 3.1). As a consequence of using the coupling circuit, the voltage applied to the plasma is lower than the input voltage of the source when conduction is present. The series resistance, often called ballast resistance, is adjusted for each simulation empirically since the equivalent resistance of the plasma is unknown prior the simulation.

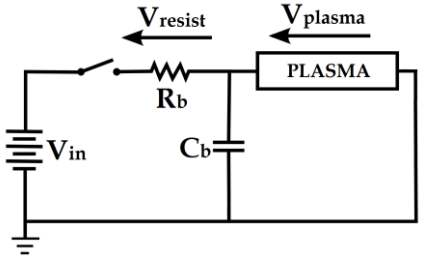

Figure 3.1: RC series coupling circuit

The proposed EHD thruster geometry presents axisymmetry around the vertical axis and is composed by an anode rod and conical cathode (The simulation region consists of a 2D cut plane of the model) as depicted in Figure 3.2.

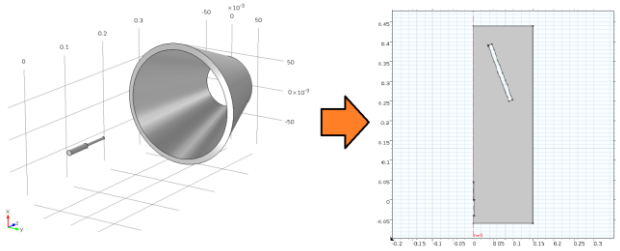

Figure 3.2: Simulation region

3.1. Argon kinetic model

Most of the argon electron impact reactions have been reported in terms of cross section data (see [9]), in such cases equation (2) is used to determine the correspondent reaction rate coefficient. Table 3.1 shows the electron impact and chemical reaction used on the present model. The species Ar* represents a metastable grouping of ten 4p states ($2p_{1-10}$ in Paschen notation, 12.09–13.48 eV) [10].

Table 3.1: Rate coefficients for argon reactions

Reaction	Rate coefficient [m^3/s or m^6/s]	References
e-impact		
$e+Ar \rightarrow e+Ar$	σ(u)	[9]
$e+Ar \rightarrow e+Ar^*$	σ(u)	[9]
$e+Ar \rightarrow 2e+Ar^+$	σ(u)	[9]
$e+Ar^* \rightarrow 2e+Ar^+$	σ(u)	[9]
Chemical		
$Ar^*+Ar^* \rightarrow e+Ar+Ar^+$	$6.4x10^{-16}$	[1],[5]
$Ar^*+Ar \rightarrow Ar+Ar$	$2.3x10^{-21}$	[1],[5]

Both the argon excited species and its ions present interaction with the outer walls (boundary of simulation) and the electrodes: Metastable argon atoms revert to the ground state with a certain probability (sticking coefficient) and ions get neutralized when hitting both the walls and the anode but when hitting the cathode they also release secondary electrons (See Table 3.2).

Table 3.2: Surface reactions for argon

Reaction	Surface†	Sticking coefficient γ_f	Secondary emission coefficient γ_i
$Ar^* \rightarrow Ar$	W, A, C	1	0
$Ar^+ \rightarrow Ar$	W, A	1	0
$Ar^+ \rightarrow Ar$	C	1	0.25

†W: Walls, A: Anode, C: Cathode.

The simulation conditions considered in the present work include: V_{in}=125 V, R_b=20 kΩ, C_b=1 pF, p_0=0.5 Torr and T_0=300 K.

4. Numerical results

Voltages of the elements of the circuit are plotted against simulation time in Figure 4.1(a). As stated in Section 3, $\mathbf{V_{plasma}}$ depicts the resultant voltage applied to the electrodes of the thruster and does not reach the $\mathbf{V_{in}}$ value since there is a voltage drop in the ballast resistance due to current flow in the circuit as seen in Figure 4.1(b).

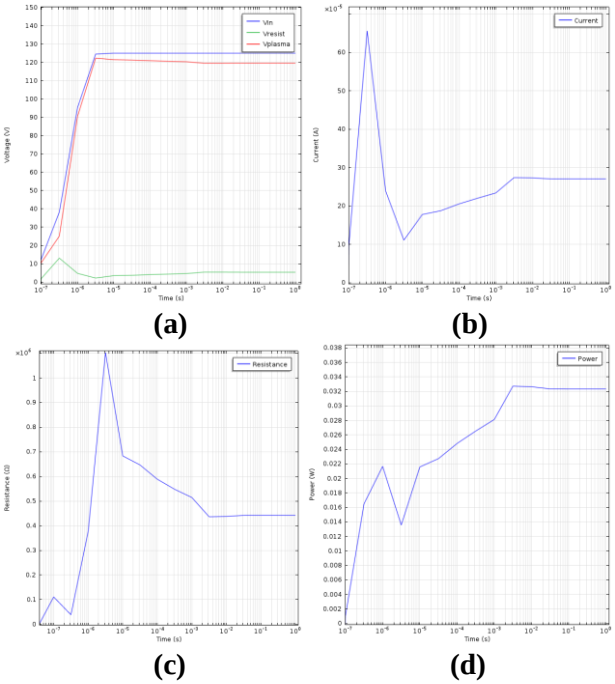

Figure 4.1: (a) Voltages in coupling circuit, (b) current flowing between electrodes, (c) equivalent resistance of plasma and (d) power expenditure in plasma.

The plasma presents an equivalent resistance during the discharge so that the power spent by the thruster varies during the discharge as well given the current and resistance profile, Figure 4.1 (b) to (d), but they all reach stable values at the end of the simulation because the stationary regime is attained. The thruster consumes typically 32 mW of power at 120 V.

As shown in Figure 4.2 (a) and (c), electrons tend to accumulate in the region of high electric potential because they are attracted by the electric field as can be seen in Figure 4.3(a), and there they have a high probability to ionize the neutral argon atoms. Electron density peaks in the center region at $1.28x10^{14}$ m^{-3}.

The excited state Ar* is also produced in majority in the same region through the inelastic

process with electrons (e+Ar→e+Ar*) from where they diffuse (See Figure 4.2(d)).

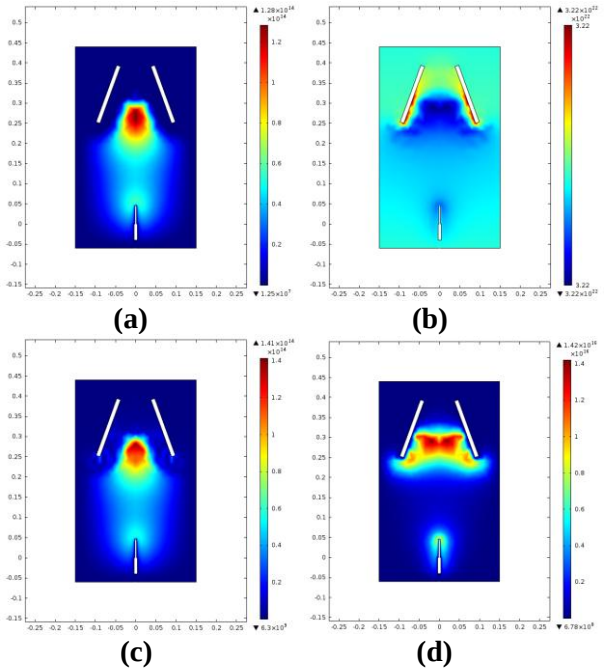

(a) **(b)**

(c) **(d)**

Figure 4.2: (a) Electron density and number densities of (b) Ar, (c) Ar^+ and (d) Ar*. All units in number of particles per m^3.

It seems that secondary emitted electrons cannot acquire immediately their maximum temperature because they face a boundary of higher neutral species concentration where they lose energy due to elastic collisions. Ground state argon and excited argon are more significantly present at the inner edge of the cathode walls, pressing against it and even been released by the end of the thruster as seen in Figure 4.2 (b) and (d).

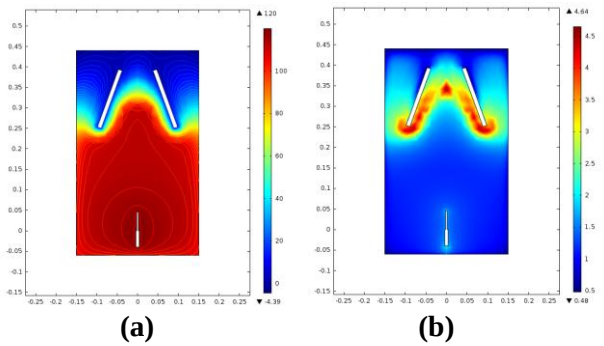

(a) **(b)**

Figure 4.3: (a) Electric potential distribution (V) with contour lines and (b) electron temperature (eV).

The electron temperature (Figure 4.3(b)) tends to be higher (4.64 eV) near the cathode region where the electric field is higher as well, as can be seen from the variation of the electric potential in Figure 4.3(a). The electric potential variation is nonlinear due to the presence of the plasma. The cathode is emitting secondary electrons due to ion bombardment and they are submitted to stronger electric field pointing at the center of the thruster as soon as they are extracted.

As can be seen in Figure 4.4(a), the gas flow shows vortex formations both inside and outside the thruster as well as laminar flow in the region between the anode and the cathodes. The top speed is given near the first contact surface of the air coming from the anode towards the cathode at 0.2 cm/s. In Figure 4.4(b) we see the pressure differential, which follows the neutral concentration profile (compare with Figure 4.2(b)).

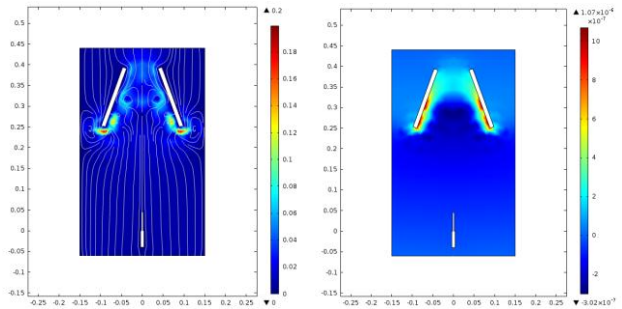

(a) **(b)**

Figure 4.4: (a) Velocity magnitude (cm/s) including flow lines and (b) pressure differential with respect to initial pressure ($p-p_0$) (Torr).

5. Conclusions

It is possible to simulate different configurations of EHD thrusters if considered a self-consistent set of reactions and proper boundary conditions. Once a first model using argon gas is proven consistent, other gases and pressures can be explored for a wider study on the matter as we are currently conducting with nitrogen and oxygen (an electronegative gas).

Geometric configuration of the thruster is not yet optimized as we can conclude from the low velocity profile obtained (maximum of 0.2 cm/s) near the entrance of the cathode region. The main reason for this behaviour is due to the poor momentum transfer from ions and electrons to neutrals, because they seem to be imprisoned in a region without any further movement.

Argon gas at low pressure presents a poor energy conversion mechanism as seen by the low air flow velocity but consists of an appropriate first approach when simulating DC discharges due to the low amount of e-impact and chemical reactions needed.

The next phase of our work will be the optimization of the geometry in terms of energy conversion and the use of better materials to improve the generation of secondary electrons emitted by the cathode. As it is well known, argon is

not a good momentum transfer medium and we plan to investigate other gas mediums such as nitrogen, oxygen and a mixture of both [6]. Preliminaries results show that in a low pressure nitrogen discharge the maximum value of the velocity profile attains about 15 cm/s, almost two orders of magnitude higher than in the case of argon, as presented here.

6. References

[1] A. Bogaerts and R. Gijbels, Modeling of metastable argon atoms in a direct-current glow discharge, *Physical Review A*. **52** (1995).

[2] A. Ieta and R. Ellis, Characterization of corona wind in a modular electrode configuration, *Proc. ESA Annual Meeting on Electrostatics* (2013).

[3] N. E. Jewell-Larsen, S. V. Karpov, I. A. Krichtafovitch, V. Jayanty, C. Hsu, and A. V. Mamishev, Modeling of corona-induced electrohydrodynamic flow with comsol multiphysics, *Proc. ESA Annual Meeting on Electrostatics* (2008) Paper E1.

[4] K. N. Kiousis, A. X. Moronis and E. D. Fylladitakis, Ionic wind generation during positive corona discharge in a wire-cylinder air gap, *IJESIT* **4**, Issue 1. (2015) 2319-5967.

[5] S. K. Lam, C-E Zheng, D. Lo, A. Dem'yanov and A. P. Napartovich, Kinetics of Ar^*_2 in high-pressure pure argon, *Journal of Physics D: Applied Physics* **33**, (2000) 242.

[6] A. A. Martins and M. J. Pinheiro, Modeling of an EHD corona flow in nitrogen gas using an asymmetric capacitor for propulsion, *J. Electrostat.* **69**, (2011) 133–138.

[7] A. A. Martins and M. J. Pinheiro, On the influence that the ground electrode diameter has in the propulsion efficiency of an asymmetric capacitor in nitrogen gas, *Phys. Plasmas*, **18**, (2011) 033512.

[8] K. Masuyama, Performance characterization of electrohydrodynamic propulsion devices, Master's thesis, *Massachusetts Institute of Technology*, (2012).

[9] Morgan database, www.lxcat.net, retrieved on January 25, 2015.

[10] S. Olenici-Craciunescu, A. Michels, C. Meyer, R. Heming, S. Tombrink, W. Vautz, and J. Franzke, *Spectrochim. Acta, Part B* **64**, (2009) 1253.

[11] L. Zhao, K. Adamiak, and M. Mazumder, Numerical and experimental studies of the electrohydrodynamic pump for sampling system on mars, *Proc. ESA Annual Meeting on Electrostatics*, (2008) Paper O3.